

RESSALVA

Atendendo solicitação do(a) autor(a), o texto completo desta tese será disponibilizado somente a partir de 20/10/2025.

unesp



**UNIVERSIDADE ESTADUAL
PAULISTA "JÚLIO DE MESQUITA
FILHO"**



**Instituto de Química Campus de
Araraquara**

**INVESTIGATION OF d , f , AND INTERMETALLIC
COMPLEXES AND THE STRATEGIES TO APPLY
THEM IN SOLID-STATE LIGHTING DEVICES,
OXYGEN SENSING, AND CELL LABELING STUDY**

Ph. D. Thesis

FELIPE DA SILVA MANRIQUE CANISARES

ARARAQUARA

2023

FELIPE DA SILVA MANRIQUE CANISARES

**INVESTIGATION OF *d*, *f*, AND INTERMETALLIC COMPLEXES AND
THE STRATEGIES TO APPLY THEM IN SOLID-STATE LIGHTING
DEVICES, OXYGEN SENSING, AND CELL LABELING STUDY**

**Thesis presented to the Institute of Chemistry,
São Paulo State University, to obtain the
degree of Doctor in Chemistry**

Supervisor: Prof. Dr. Sergio Antonio Marques de Lima

Co-supervisor: Prof. Dr. Marian Rosaly Davolos

ARARAQUARA

2023

FELIPE DA SILVA MANRIQUE CANISARES

**INVESTIGAÇÃO DE COMPLEXOS *d, f*, E INTERMETÁLICOS E AS
ESTRATÉGIAS PARA APLICÁ-LOS EM DISPOSITIVOS DE
ILUMINAÇÃO DE ESTADO SÓLIDO, SENSOREAMENTO DE
OXIGÊNIO, E IMAGEAMENTO CELULAR**

**Tese apresentada ao Instituto de Química,
Universidade Estadual Paulista, como parte
dos requisitos para obter o título de Doutor
em Química**

Orientador: Prof. Dr. Sergio Antonio Marques de Lima

Co-orientadora: Profa. Dra. Marian Rosaly Davolos

ARARAQUARA

2023

C223i Canisares, Felipe da Silva Manrique
Investigation of d, f, and intermetallic complexes and the strategies to apply them in solid-state lighting devices, oxygen sensing, and cell labeling study/ Felipe da Silva Manrique Canisares – Araraquara: [s.n.], 2023
166 p.: il.

Thesis (doctor) – Universidade Estadual Paulista, Instituto de Química
Advisor: Sergio Antonio Marques de Lima
Co-advisor: Marian Rosaly Davolos

1. Rare earth metals. 2. Iridium. 3. Metal complexes.
4. Photoelectronic devices. 5. Aqueous dissolved oxygen.
I. Title.

Sistema de geração automática de fichas catalográficas da Unesp. Biblioteca do Instituto de Química, Araraquara. Dados fornecidos pelo autor(a).

Essa ficha não pode ser modificada

CERTIFICADO DE APROVAÇÃO

TÍTULO DA TESE: "Investigation of d, f, and intermetallic complexes and the strategies to apply them in solid-state lighting devices, oxygen sensing, and cell labeling study"

AUTOR: FELIPE DA SILVA MANRIQUE CANISARES

ORIENTADOR: SERGIO ANTONIO MARQUES DE LIMA

COORIENTADORA: MARIAN ROSALY DAVOLOS

Aprovado como parte das exigências para obtenção do Título de Doutor em Química, pela Comissão Examinadora:

Prof. Dr. SERGIO ANTONIO MARQUES DE LIMA (Participação Virtual)
Departamento de Física, Química e Biologia / Faculdade de Ciências e Tecnologia - Unesp/ Câmpus de Presidente Prudente


Prof. Dr. HERMI FELINTO DE BRITO (Participação Virtual)
Departamento de Química Fundamental / Universidade de São Paulo - USP - São Paulo

Prof. Dr. VERA REGINA LEOPOLDO CONSTANTINO (Participação Virtual)
Departamento de Química Fundamental / Instituto de Química - USP - São Paulo

Prof. Dr. ROBERTO SANTANA DA SILVA (Participação Virtual)
Departamento de Física e Química / Faculdade de Ciências Farmacêuticas - USP - Ribeirão Preto

Prof. Dr. SIDNEY JOSE LIMA RIBEIRO (Participação Virtual)
Química Analítica, Físico-Química e Inorgânica / Instituto de Química - UNESP - Araraquara

Araraquara, 20 de outubro de 2023

Documento assinado digitalmente
 SERGIO ANTONIO MARQUES DE LIMA
Data: 26/10/2023 17:38:56-0300
Verifique em <https://validar.iti.gov.br>

PORTARIA UNESP No 117, DE 21 DE DEZEMBRO DE 2022.
INSTRUÇÃO AT/PROPG No 02, DE 22 DE DEZEMBRO DE 2022.

IMPACTO POTENCIAL DESTA PESQUISA

Os potenciais impactos decorrentes desta tese compreendem o aprofundamento do processo de sensibilização em complexos heterobimetálicos de Ir^{III} e Eu^{III}, tanto em ambiente rígido quanto em solução, além de possibilitar o desenvolvimento de dispositivos altamente eficientes no processo de conversão de energia. Tais materiais apresentam potencial para aplicação como dispositivos de iluminação de estado sólido, e sensores luminescentes eficientes na aferição de oxigênio dissolvido, o qual pode servir como poderoso diagnóstico de cânceres em estágios iniciais. Desta forma, as contribuições aqui apresentadas potencialmente influenciarão pesquisas voltadas a beneficiar variados setores da sociedade moderna, como as ciências da vida, energia e meio ambiente.

POTENTIAL IMPACT OF THIS RESEARCH

The potential impacts resulting from this thesis include the understanding of the sensitization process in Ir^{III}-Eu^{III} heterobimetallic complexes, both in a rigid environment and in solution, in addition to enabling the development of highly efficient devices in the energy conversion process. Such materials have the potential for application as solid-state lighting devices and efficient luminescent sensors for measuring dissolved oxygen, which could serve as powerful diagnostic tools for early-stage cancers. Therefore, the contributions presented here can influence research that benefits various sectors of modern society, such as life sciences, energy, and the environment.

DATA

Personal information

Full name: Felipe da Silva Manrique Canisares

Name in bibliography Citation: CANISARES, F. S. M.; CANISARES, FELIPE S.M.; CANISARES, F.S.M.; CANISARES, FELIPE S. M.

Nationality: Brazilian

Birth city: Martinópolis, São Paulo, Brazil

Profession: Chemist

Adress: Instituto de Química – Universidade Estadual Paulista “Júlio de Mesquita Filho” – Av. Francisco Degni, 55 – Jardim Quintandinha – Araraquara – SP

CEP: 14800-060

e-mail: manrique.canisares@unesp.br

Academic education

2012 - 2016: São Paulo State University (Unesp), School of Technology and Sciences, Presidente Prudente, Chemistry

2017 - 2019: São Paulo State University (Unesp), Institute of Biosciences, Humanities and Exact Sciences, São José do Rio Preto, Master of Sciences in Chemistry (Advisor: Prof. Sergio A. M. de Lima)

2022 - 2023: Visiting Scholar at University of Southern California, Fulbright Fellow (Advisor: Prof. Mark E. Thompson)

Professional Experience

2020 – 2022: Collaborating professor, Biochemistry, São Paulo State University (Unesp), School of Technology and Sciences

Awards

2022: Doctoral Dissertation Research Award (DDRA), Fulbright Commission

2016: Honorable Mention at the XXVIII CIC UNESP as one of the best works presented in the Exact Sciences area.

2016: Best Poster Award presented at the XVIII BMIC - Brazilian Meeting on Inorganic Chemistry and 7th Brazilian Meeting on Rare Earths (XVIII BMIC + TR)

2015: Best paper presented in the Inorganic Chemistry Division at 38th Annual Meeting of the Brazilian Chemical Society, SBQ.

Published scientific articles

1. MUTTI, ALESSANDRA M. G.; **CANISARES, FELIPE S. M.** SANTOS, JOÃO A. O.; SANTOS, BRUNO C.; CAVALCANTE, DALITA G. S. M.; JOB, ALDO E.; PIRES, ANA M.; LIMA, SERGIO A. M. Silica-based nanohybrids containing europium complexes covalently grafted: structural, luminescent, and cell labeling investigation JOURNAL OF SOL-GEL SCIENCE AND TECHNOLOGY, v. 106, p. 10971-023-06138, 2023.
2. BELTRAME, ARIANE C. F.; BISPO-JR, AIRTON G.; **CANISARES, FELIPE S. M.**; FERNANDES, RICARDO V.; LAURETO, EDSON LIMA, SERGIO A. M.; PIRES, ANA M. PMMA or PVDF films blended with β -diketonate tetrakis Eu III or Tb III complexes used as downshifting coatings of near-UV LEDs, v. 19, p. 3992-4000, 2023.
3. SILVA, RENAN C.; **CANISARES, FELIPE S.M.**; MUTTI, ALESSANDRA M.G.; PIRES, ANA M.; LIMA, SERGIO A.M. Small Schiff base molecules derived from salicylaldehyde as colorimetric and fluorescent neutral-to-basic pH sensors. DYES AND PIGMENTS, v. 213, p. 111191, 2023.
4. **CANISARES, FELIPE S. M.**; MUTTI, ALESSANDRA M. G.; SANTANA, EDY F.; OLIVEIRA, VYTOR C.; CAVALCANTE, DALITA G. S. M.; JOB, ALDO E.; PIRES, ANA M.; LIMA, SERGIO A. M. Red-emitting heteroleptic iridium(III) complexes: photophysical and cell labeling study. PHOTOCHEMICAL SCIENCES (ONLINE), v. 21, p. 1077-1090, 2022.
5. **CANISARES, FELIPE S.M.**; MUTTI, ALESSANDRA M.G.; CAVALCANTE, DALITA G.S.M.; JOB, ALDO E.; PIRES, ANA M.; LIMA, SERGIO A.M.

Luminescence and cytotoxic study of red emissive europium(III) complex as a cell dye. JOURNAL OF PHOTOCHEMISTRY AND PHOTOBIOLOGY A-CHEMISTRY, v. 422, p. 113552, 2021.

6. MUTTI, A.M.G.; **CANISARES, F.S.M.**; MACHINI, W.B.S.; PIRES, A.M.; TEIXEIRA, M.F.S.; LIMA, S.A.M. A spectroscopic experimental and semi-empirical study of [Eu(salen)₂] as a red-emitter for phosphor-converted UV LED. OPTIK, v. 243, p. 167454, 2021.
7. **CANISARES, FELIPE S.M.**; BISPO, AIRTON G.; PIRES, ANA M.; LIMA, SERGIO A.M.; Syntheses and characterization of Schiff base ligands and their Ir(III) complexes as coating for phosphor-converted LEDs. OPTIK, v. 219, p. 164995, 2020.
8. LEITE SILVA, CAMILA M.B.; BISPO'JR, AIRTON G.; **CANISARES, FELIPE S.M.**; CASTILHO, SHIRLEY A.; LIMA, SERGIO A.M.; PIRES, ANA M.; Eu³⁺ - tetrakis β-diketonate complexes for solid-state lighting application. LUMINESCENCE, v. 34, p. 877-886, 2019.

Submitted scientific articles

1. **CANISARES, FELIPE S.M.**, SILVA, R.C., DAVOLOS, M.R., PIRES, A.M., LIMA, S.A.M., Heterobimetallic Iridium^{III}-Europium^{III} complex: The role of donor energy on sensitising the Eu^{III} ion. NEW JOURNAL OF CHEMISTRY.
2. SILVA, R.C., **CANISARES, FELIPE S.M.**, SARAIVA, L.F., PIRES, A.M., LIMA, S.A.M., Featuring long-lifetime deep-red emitting iridium^{III} complexes with high colour purity: insights on the excited state dynamics from spectroscopic and theoretical perspectives. DALTON TRANSACTIONS.

I dedicate this thesis to my parents Oswaldo and Vera Lúcia.

Acknowledgments

First, I want to thank God for all the wonders He has done and continues to do in my life, for being always with me, whether in good or bad moments. For giving me his infinite Grace, for giving me all his love, for giving me the strength to move forward, no matter the obstacles in the way. I am also grateful for the people He has placed in my life. I thank Our Lady and all the saints for always interceding for me with God.

To my parents Vera Lúcia and Oswaldo, my sister Vanessa, and my brother Bruno for always supporting me and believing in me. To all my family, and all the friends I consider part of the family, for always rooting for me. Especially to Ana Maria, Francine, Kaliani, Nataly, and Vanessa, those who believe in and use education as a tool to transform lives.

To Professor Sergio Antonio Marques de Lima for his guidance and all his teachings, which were fundamental to the development of this work.

To Professor Ana Maria Pires for all her contributions to my work, teaching, and friendship. And for being one of the most human people I have met.

I sincerely appreciate all my lab-mates of the LLuMeS, Airton, Alessandra, Alessandro, André, Ariane, Augusto, Bianca, Bruno, Caique, Camila, Danúbia, Edy, Filipe, Gustavo, João, Leonardo, Luis, Maísa, Maria Eduarda, Nagyla, Paloma, Rebeca, Renan, Rodolpho, and Vytor, with whom I shared good moments, experiences, and knowledge. A special thank you to Edy who, throughout my scientific initiation period, had the patience to co-supervise me. To the undergrad students Vytor, and Augusto for their great assistance in the synthesis and purification processes of ligands and complexes. To Renan for his collaborative work related to iridium compounds. To Alessandra for the scientific collaboration in recent years, in which we published beautiful articles. To Ariane for her friendship and scientific collaboration over the last few years, who brought Axé's joy to the lab. To João Antonio for his help with biological assays. To Alessandro for help with photophysical measurements.

I am immensely grateful to my “prudentina” family, Shirley, Tamy, and Andressa, for the days of distraction, lots of noise, music, and cooking classes

(unfortunately I didn't learn). I mainly thank Andressa, with whom I spent the last years of my doctorate, and we shared such good memories.

To my friends from the Chemistry course at FCT-UNESP, with whom I was with every day for 5 years: Thais, Bruno, João, Alessandro, Nathalia, Matheus, Miriam, Aline, and Ricardo.

To Professor Aldo Eloiso Job from FCT-UNESP for the use of his laboratories and collaboration in the development of the project.

To the Fulbright Commission for the opportunity to develop part of my research in one of the most important research groups on luminescent materials. Especially to Carol, who was always very kind throughout the selection process and the internship period in the United States. To all the Fulbrighters in the 2022–2023 cohort, especially Fernanda, Isis, and Sabrina, the Southern California Fulbrighters, who shared great times with me during this time.

To Professor Mark Edward Thompson for opening his laboratory at the University of Southern California (USC) and for the knowledge acquired. To Peter Djurovich for the hours of conversations, which were fundamental in resolving the problems that arose during the development of the project. To Judy Fong, who was very receptive from the first moment I entered the laboratory. To Mattia and Michela, the most Brazilian Italians I know, who made my adaptation process in the United States a little easier. To Mattia and James, with whom I shared hood 3 during my internship. And to all the amazing people I have had the pleasure of meeting and working with: Kelly, Marsel, Allen, Gemma, Jonas, Junru, Collin, Megan, Ao, Konstantin, Nina, Chandler, Francis, Sunil, Eric, Jie, Austin, Mahsa, Caleb, and Sarah.

To the teachers who supported me in getting here, from primary education to postgraduate courses. I am extremely grateful to the Institute of Chemistry of the São Paulo State University and to the professors who directly or indirectly influenced my Ph. D studies, especially Professor Marian Rosaly Davolos, for opening the doors of her laboratory and for the support provided during the development of this work.

This study was financed in part by the Coordenação de Aperfeiçoamento de Pessoal de Nível Superior – Brasil (CAPES) – Finance code 001.

RESUMO

A redução do consumo energético por dispositivos de iluminação e imagem, assim como a eficácia na detecção e diagnóstico de doenças por técnicas de imageamento, passa pelo desenvolvimento de materiais emissivos com alta eficiência de emissão. Em ambas as áreas de aplicação, luminóforos vermelhos são de grande interesse, já que por ora podem compor o sistema RGB, possibilitando a geração de qualquer cor luz, inclusive a sensação de luz branca, e ora porque em ensaios biológicos a emissão vermelha distingue-se da autofluorescência do tecido celular, que normalmente ocorre na região do azul ao verde, além da luz vermelha ser menos absorvida pelo sangue, gordura e pele. Complexos emissivos no vermelho com alta pureza da cor são facilmente obtidos através da utilização do íon Eu^{III} , o qual possui bandas estreitas de emissão, todavia, embora os emissores vermelhos baseados no íon Eu^{III} tenham alta pureza de cor, o Φ é tipicamente menor do que emissores baseados em metais do bloco *d*. Estrategicamente, a síntese de complexos heterobimetálicos *d-f*, combinando o alto Φ dos complexos do bloco *d* com a alta pureza de cor dos íons lantanídeos tem sido explorada. Neste contexto, novos sistemas utilizando os íons Ir^{III} e Eu^{III} foram sintetizados e estudados, tendo como foco a compreensão do processo de sensibilização ao íon Eu^{III} em sistemas bimetálicos, assim como estudar as estratégias para aplicá-los em dispositivos de iluminação de estado sólido, no sensoreamento de oxigênio dissolvido, e em imageamento celular. Duas abordagens para sintetizar complexos heterolépticos de Ir^{III} foram estudadas, objetivando obter complexos com diferentes arranjos (*cis* e *trans*), ficando evidente que os diferentes arranjos influenciam nas propriedades fotofísicas dos complexos. Dois novos complexos bimetálicos $\text{Ir}^{\text{III}}\text{-Ln}^{\text{III}}$ ($\text{Ln}^{\text{III}} = \text{Gd}^{\text{III}}$ ou Eu^{III}) foram estudados, e mostraram que o processo de sensibilização ao íon Eu^{III} não é estritamente dependente da diferença energética entre o estado doador e o estado emissor ($^5\text{D}_0$) quando em solução, já que mesmo que o estado doador $^3\text{MLCT}$ esteja situado em região de baixa energia, a sensibilização é um processo favorável quando medido em solventes com alta polaridade. O complexo heterobimetálico de $\text{Ir}^{\text{III}}\text{-Eu}^{\text{III}}$ foi imobilizado em filmes de PMMA e aplicado na fabricação de protótipos do tipo LED recoberto, objetivando aplicação em iluminação de estado sólido. Através da modulação da voltagem aplicada ao chip LED UV utilizado como fonte de

excitação, determinou-se que a energia mínima do nível doador $^3\text{MLCT}$ para observar apenas a emissão vermelha do íon Eu^{III} é de 19.103 cm^{-1} . Por fim, partículas de sílica decoradas com complexos de $\text{Ir}^{\text{III}}\text{-Eu}^{\text{III}}$ foram estudadas na detecção de oxigênio dissolvido. As medições na detecção de oxigênio mostraram que o híbrido final tem uma resposta não-linear com sensibilidade de 70,5%. Os testes de toxicidade foram realizados utilizando células Huh-7.5 e as nanopartículas $\text{SiO}_2\text{-Eu}^{\text{III}}\text{Ir}^{\text{III}}$ foram atóxicas em concentrações entre $1,56$ e $400 \mu\text{g}\cdot\text{mL}^{-1}$. Através de microscopia confocal foi comprovado que as nanopartículas foram internalizadas pelas células mantendo suas propriedades luminescentes, habilitando-as como sondas para imageamento celular.

Palavras-chave: lantanídeo; irídio; complexo heterobimetálico; iluminação de estado sólido; sensoreamento de oxigênio.

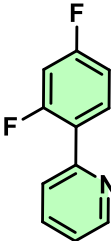
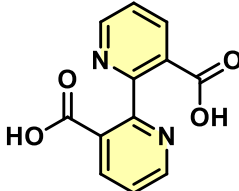
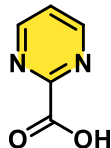
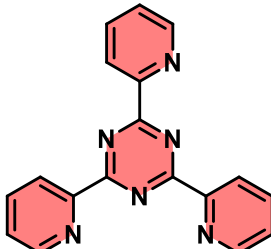
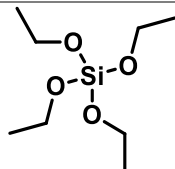
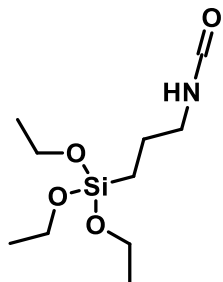
ABSTRACT

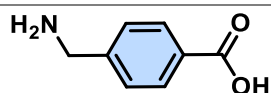
To reduce the energy consumption of lighting and imaging devices, as well as to increase the effectiveness to detect and to diagnose diseases through imaging techniques, involves the development of emissive materials with high emission efficiency. In both areas of application, red luminophores are of great interest because they can compose the RGB system, enabling the generation of light of any color, including the sensation of white light, and because in biological tests, the red emission is distinguished from the autofluorescence of cellular tissue, which normally occurs in the blue to green region. In addition, red light is less absorbed by blood, fat, and skin. Red emissive complexes with high color purity are easily obtained using the Eu^{III} ion, which have narrow emission bands. However, although red emitters based on the Eu^{III} ion have high color purity, Φ is typically lower than that of emitters based on d -metal complexes. Strategically, the synthesis of heterobimetallic d - f complexes, combining the high Φ of d -metal complexes with the high color purity of lanthanide ions, has been explored. In this context, new systems using Ir^{III} and Eu^{III} ions were synthesized and studied, with a focus on understanding the sensitization process to Eu^{III} ion in bimetallic systems, as well as studying strategies to apply them in solid-state lighting devices, dissolved oxygen, and cell imaging. Two approaches for the synthesis of heteroleptic Ir^{III} complexes were studied, aiming to obtain complexes with different arrangements (*cis* and *trans*). It became evident that the different arrangements influence the photophysical properties of the complexes. Two new bimetallic complexes $\text{Ir}^{\text{III}}\text{-Ln}^{\text{III}}$ ($\text{Ln}^{\text{III}} = \text{Gd}^{\text{III}}$ or Eu^{III}), were studied and showed that the sensitization process to the Eu^{III} ion is not strictly dependent on the energetic difference between the donor state and the emitter state ($^5\text{D}_0$) when in solution, since when the $^3\text{MLCT}$ donor state is in a low-energy region, sensitization is a favorable process if in solvents with high polarity. The $\text{Ir}^{\text{III}}\text{-Eu}^{\text{III}}$ heterobimetallic complex was immobilized in PMMA films and used in the manufacture of coated LED prototypes, aiming for application in solid state lighting. By modulating the voltage applied to the UV LED chip used as an excitation source, it was determined that the minimum energy of the $^3\text{MLCT}$ donor level to observe only the red emission of the Eu^{III} ion in a rigid system is $19,103\text{ cm}^{-1}$. Finally, silica particles decorated with $\text{Ir}^{\text{III}}\text{-Eu}^{\text{III}}$ complexes were studied for the detection of dissolved oxygen. Oxygen detection measurements

showed that the final hybrid has a non-linear response with a sensitivity of 70.5%. Toxicity tests were performed using Huh-7.5 cells, and SiO₂-Eu^{III}Ir^{III} nanoparticles were found to be nontoxic at concentrations between 1.56 and 400 µg·mL⁻¹. Through confocal microscopy, it was proven that the nanoparticles were internalized by cells while maintaining their luminescent properties, making them promising candidates as probes for cellular imaging.

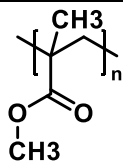
Keywords: lanthanides; iridium; heterobimetallic complex; solid state lighting; oxygen sensing

List of ligands and polymers

Structure	Name (Abbreviation)
	2-(2,4-difluorophenyl)pyridine (dfppy)
	2,2'-bipyridine-3,3'-dicarboxylic acid (bpdc)
	Pyrimidine-2-carboxylic acid (pmc)
	2,4,6-tris(2-pyridyl)-s-triazine (tptz)
	Tetraethyl orthosilicate (TEOS)
	3-(triethoxysilyl)propyl isocyanate (IPTES)



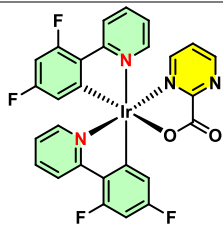
4-(aminomethyl)benzoic acid (abac)



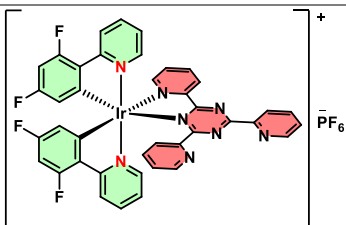
Poly(methyl methacrylate) (PMMA)

Molecules and particles synthesized in this study

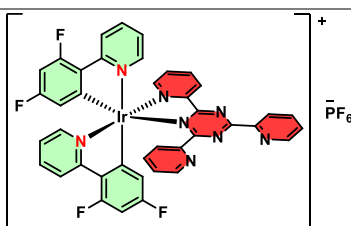
Structure	Abbreviation
	[(dfppy) ₂ Ir(μ-Cl) ₂ Ir(dfppy) ₂]
	N,N- <i>trans</i> -[Ir(dfppy) ₂ (bpdc)], N,N-(<i>trans</i>)-Ir ^{III} p, or Ir ^{III} -p
	N,N- <i>cis</i> -[Ir(dfppy) ₂ (bpdc)], or N,N-(<i>cis</i>)-Ir ^{III} p
	N,N- <i>trans</i> -[Ir(dfppy) ₂ (pmc)], or N,N-(<i>trans</i>)-Ir ^{III} m



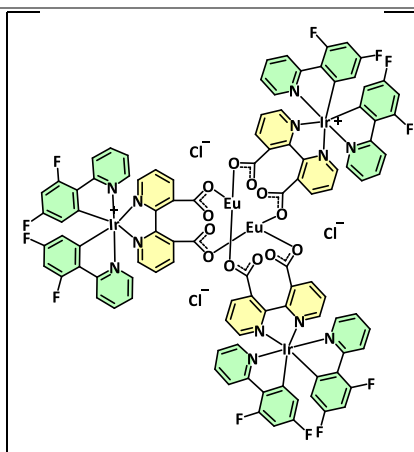
**N,N-*cis*-[Ir(dfppy)₂(pmc)], or
N,N-(*cis*)-Ir^{III}m**



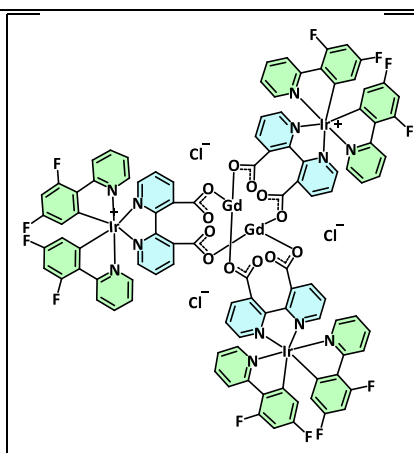
**N,N-*trans*-[Ir(dfppy)₂(tptz)], or
N,N-(*trans*)-Ir^{III}t**



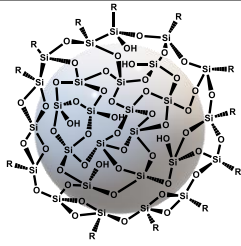
**N,N-*trans*-[Ir(dfppy)₂(tptz)], or
N,N-(*cis*)-Ir^{III}t**



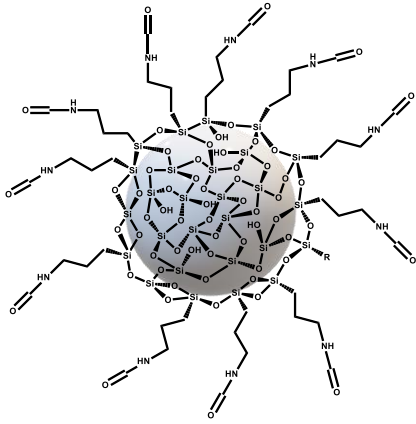
**[{Ir(dfppy)₂(μ-bpdc)}₃Eu₂]Cl₃·nH₂O·mCH₃OH
Ir^{III}-Eu^{III}**



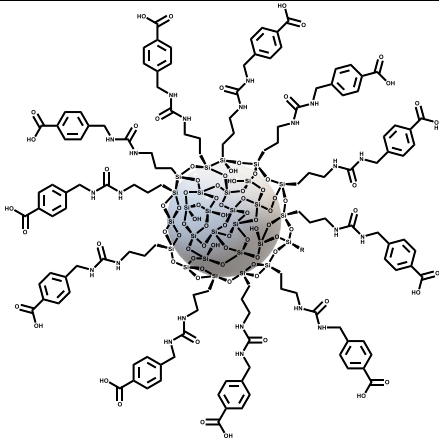
**[{Ir(dfppy)₂(μ-bpdc)}₃Gd₂]Cl₃·nH₂O·mCH₃OH
Ir^{III}-Gd^{III}**



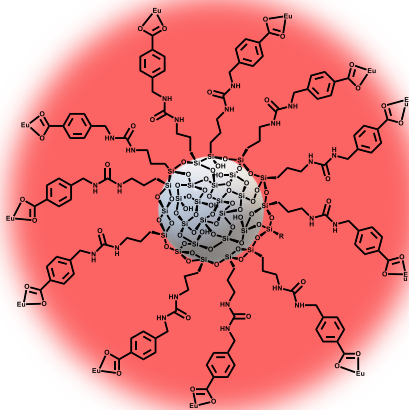
SiO₂



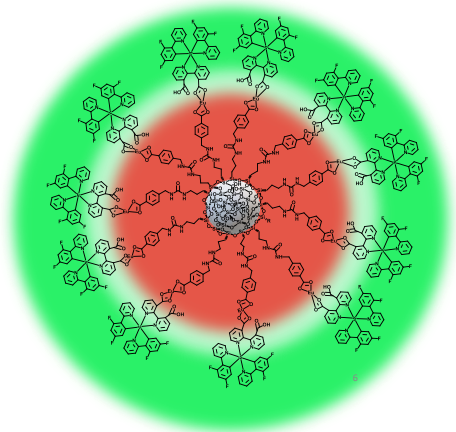
SiO₂-NCO



SiO₂-COOH



SiO₂-COOEu^{III}



SiO₂-COOEu^{III}-Ir^{III}

* For simplicity, only the Δ stereoisomer of the six complexes and Ir^{III}-dimer precursor are represented here, however the classic Nonoyama route lead to a racemic mixture of both Δ and Λ stereoisomers.

** The molecules grafted onto silica particles are out of scale, and merely represent an illustration of the formation of the hybrid.

List of figures

- Figure 1.** Emission spectra of selected trivalent lanthanide ions.38
- Figure 2.** Partial energy diagram of Eu^{III} ($4f^6$) showing the relative magnitudes of interelectronic repulsion (terms), spin–orbit coupling (levels), and crystal-field effects (sublevels). On the right side, the emission spectrum of Eu^{III} ion in the $[\text{Eu}(\text{salen})_2]$ complex is presented. The complex structure is also inserted [].39
- Figure 3.** Schematic and simplified molecular orbital diagram for an octahedral d^6 metal complex involving 2-phenylpyridine (ppy) (C_3 symmetry)-type ligands, in which various possible transitions are indicated. On the right side, the emission spectrum of $[\text{Ir}(\text{ppy})_3]$ complex is presented, and the complex structure is also inserted. Adapted from [50].42
- Figure 4.** Energy transfer between Ir^{III} complex and Eu^{III} in a bimetallic system.44
- Figure 5.** The triplet energy of Ir^{III} complexes used to sensitize the Eu^{III} ion in $\text{Ir}^{\text{III}}\text{-Eu}^{\text{III}}$ heterobimetallic complexes found in the literature.45
- Figure 6.** a) Representation of the sum of spins used to determine the spin multiplicity; b) representation of spin angular momentum vectors, s_1 and s_2 equal $\frac{1}{2}$ to obtain possible values of quantum numbers s' and m'_s . Source: Adapted from [].56
- Figure 7.** A) The OLED multilayer structure and (B) a scheme of the OLED multilayer energy diagram.57
- Figure 8.** Trans and cis isomers of iridium complexes reported in the literature. A) trans and cis $\text{N,N-}[\text{Ir}(\text{2-phenylpyridine})_2(\text{2-carboxy-4-dimethyl amino pyridine})]$ (N984) [116]; B) trans and cis $\text{N,N-}[\text{Ir}(\text{dfppy})_2(\text{dfbdpH})\text{Cl}]$ [117]; C) trans and cis $\text{N,N-}[\text{Ir}(\text{dfptrBz})_2(\text{dmbpy})]^+$ ($\text{dmbpy} = 4,40\text{-dimethyl-2,20-bipyridine}$) [118]; and D) trans and cis $\text{C,C-}[\text{Ir}(\text{Ph-Im})_2(\text{dmbpy})]^+$ ($\text{Ph-Im} = 3\text{-Methyl-1-phenyl-1H-imidazol-3-ium}$) [119].59
- Figure 9.** Ir^{III} -based complexes synthesized in this chapter.61
- Figure 10.** FTIR spectra of the bpdC ligand (black), $\text{N,N-trans-Ir}^{\text{III}}\text{p}$ (blue), $\text{N,N-cis-Ir}^{\text{III}}\text{p}$ (red), and the precursor dimer $[(\text{dfppy})_2\text{Ir}(\mu\text{-Cl})_2\text{Ir}(\text{dfppy})_2]$ (green). .65
- Figure 11.** FTIR spectra of the pmc ligand (black), $\text{N,N-trans-Ir}^{\text{III}}\text{m}$ (blue), $\text{N,N-cis-Ir}^{\text{III}}\text{m}$ (red), and the precursor dimer $[(\text{dfppy})_2\text{Ir}(\mu\text{-Cl})_2\text{Ir}(\text{dfppy})_2]$ (green). 66

- Figure 12.** FTIR spectra of pmc ligand (green), N,N-trans-Ir^{III}t (blue), N,N-cis-Ir^{III}t (red), and the precursor dimer [(dfppy)₂Ir(μ-Cl)₂Ir(dfppy)₂] (black).....67
- Figure 13.** MALDI spectra of N,N-trans-Ir^{III}p (black), N,N-cis-Ir^{III}p (red), N,N-trans-Ir^{III}m (green), N,N-trans-Ir^{III}t (purple), and N,N-cis-Ir^{III}t (wine).68
- Figure 14.** Optimized structures of (A) N,N-trans-Ir^{III}p and (B) N,N-cis-Ir^{III}p at the r²SCAN-3c/Def2-TZVP level. Grey = carbon, white = hydrogen, green = fluor, blue = nitrogen, and orange = iridium.69
- Figure 15.** Molecular orbitals of N,N-trans-Ir^{III}p. (A) HOMO-1, (B) HOMO, (C) LUMO, (D) LUMO+1, (E) LUMO+2. The isosurface was considered with a value of 0.04 e/a₀³.70
- Figure 16.** Molecular orbitals of N,N-cis-Ir^{III}p. (A) HOMO-1, (B) HOMO, (C) LUMO, (D) LUMO+1, (E) LUMO+2. The isosurface was considered with a value of 0.04 e/a₀³.70
- Figure 17.** Optimized structures of (A) N,N-trans-Ir^{III}m and (B) N,N-cis-Ir^{III}m at the r²SCAN-3c/Def2-TZVP level. Grey = carbon, white = hydrogen, green = fluor, blue = nitrogen, and orange = iridium.71
- Figure 18.** Molecular orbitals of N,N-trans-Ir^{III}m. (A) HOMO-2, (B) HOMO-1, (C) HOMO, (D) LUMO, (E) LUMO+1, (F) LUMO+3. The isosurface was considered with a value of 0.04 e/a₀³.72
- Figure 19.** Molecular orbitals of N,N-cis-Ir^{III}m. (A) HOMO-2, (B) HOMO-1, (C) HOMO, (D) LUMO, (E) LUMO+1, (F) LUMO+3. The isosurface was considered with a value of 0.04 e/a₀³.72
- Figure 20.** Optimized structures of (A) N,N-trans-Ir^{III}t and (B) N,N-cis-Ir^{III}t at the r²SCAN-3c/Def2-TZVP level. Grey = carbon, white = hydrogen, green = fluor, blue = nitrogen, and orange = iridium.73
- Figure 21.** Molecular orbitals of N,N-trans-Ir^{III}t. (A) HOMO-3, (B) HOMO-2, (C) HOMO, (D) LUMO, (E) LUMO+1, (F) LUMO+2. The isosurface was considered with a value of 0.04 e/a₀³.73
- Figure 22.** Molecular orbitals of N,N-cis-Ir^{III}t. (A) HOMO-3, (B) HOMO-2, (C) HOMO, (D) LUMO, (E) LUMO+1, (F) LUMO+2. The isosurface was considered with a value of 0.04 e/a₀³.74
- Figure 23.** Theoretical (dashed) and experimental (continuous) absorption and emission spectra of A) and B) N,N-(trans-cis)-Ir^{III}p; C) and D) N,N-(trans-cis)-Ir^{III}m; and E) and F) N,N-(trans-cis)-Ir^{III}t.75

Figure 24. Excitation and emission spectra of N,N-(trans)-Ir ^{III} p measured in different solvents.	77
Figure 25. Excitation and emission spectra of N,N-(cis)-Ir ^{III} p measured in different solvents.	77
Figure 26. Excitation and emission spectra of N,N-(trans)-Ir ^{III} m measured in different solvents.	79
Figure 27. Excitation and emission spectra of N,N-(cis)-Ir ^{III} m measured in different solvents.	80
Figure 28. Excitation and emission spectra of N,N-(trans)-Ir ^{III} t measured in different solvents.	81
Figure 29. Excitation and emission spectra of N,N-(cis)-Ir ^{III} t measured in different solvents.	81
Figure 30. Timeline representing some of the most important findings of Ir ^{III} -Ln ^{III} bimetallic systems.	89
Figure 31. Schematic illustration of potential energy transfer mechanisms in the Ir ^{III} -Eu ^{III} and Ir ^{III} -Tb ^{III} complexes. Solid, dashed, and wavy arrows represent excitation, nonradiative processes (energy transfer), and luminescence, respectively. Adapted from [154].	91
Figure 32. MALDI TOF spectrum obtained to Ir ^{III} -Eu ^{III} bimetallic complex.	94
Figure 33. A) FTIR spectra of the Ir ^{III} p, Ir ^{III} -Gd ^{III} , and Ir ^{III} -Eu ^{III} complexes, B) magnification of the region from 1350 cm ⁻¹ to 1650 cm ⁻¹	94
Figure 34. A) FTIR spectra of the Na ₂ bpdc ligand, Ir ^{III} -Gd ^{III} , and Ir ^{III} -Eu ^{III} complexes; and B) most common carboxylate coordination modes and the energy difference between $\nu_{\text{ass}}(\text{COO}^-)$ and $\nu_{\text{sym}}(\text{COO}^-)$ for each coordination mode in the complexes (Δ_{vc}) compared with the energy difference in the ligands (Δ_{vL}). To illustrate, it was used a generic carboxylic acid (benzoic acid).	95
Figure 35. A) emission spectra obtained after each addition of EuCl ₃ ; and B) graphic of the ratio of Ir ^{III} /Eu ^{III} and the energy of the maximum emission of the Ir ^{III} complex.	96
Figure 36. A) emission spectra obtained after each addition of GdCl ₃ ; and B) graphic of the ratio of Ir ^{III} /Gd ^{III} and the energy of the maximum emission of the Ir ^{III} complex.	96

- Figure 37.** Emission spectra acquired in the solid state of Ir^{III}p, Ir^{III}-Gd^{III}, and Ir^{III}-Eu^{III} complexes. All measurements were carried out with a bandpass of 2.5 nm for both Ex and Em, with an increment of 0.5 nm and an integration time of 0.5 s. The color diagram represents the energy levels of the donor state (³MLCT), and selected states of the Eu^{III} ion.97
- Figure 38.** Excitation and emission spectra of A) Ir^{III}-p; B) Ir^{III}-Gd^{III}; and C) Ir^{III}-Eu^{III} complexes in the solid state and in various solvents. Concentration in solution of 1.0x10⁻⁵ mol·L⁻¹. All measurements were carried out with a bandpass of 2.5 nm for both Ex and Em, with an increment of 0.5 nm and an integration time of 0.5 s. Some Ir^{III}-Gd^{III} emission spectra (chloroform, ethyl acetate, and acetonitrile) are contaminated with Eu^{III} ion, as can be seen by the appearance of a narrow emission band at approximately 616 nm.99
- Figure 39.** ³MLCT energy state determined using Ir^{III}-Gd^{III} complex measured in different solvents, and emission spectra acquired in chloroform, ethyl acetate, and acetonitrile solution of the Ir^{III}-Eu^{III} complex. Concentration in solution of 1.0x10⁻⁵ mol·L⁻¹. All measurements were carried out with a bandpass of 2.5 nm for both Ex and Em, with an increment of 0.5 nm and an integration time of 0.5 s. Full arrows represent favorable energy transfer, and dashed arrows partial energy transfer. 100
- Figure 40.** Excitation and emission spectra of Ir^{III}-p, Ir^{III}-Gd^{III}, and Ir^{III}-Eu^{III} complexes measured in A) ethyl acetate, B) acetonitrile, and C) DMSO. Concentration in solution of 1.0x10⁻⁵ mol·L⁻¹. All measurements were carried out with a bandpass of 2.5 nm for both Ex and Em, with an increment of 0.5 nm and an integration time of 0.5 s. 102
- Figure 41.** Excitation and emission spectra of Ir^{III}p, Ir^{III}-Gd^{III}, and Ir^{III}-Eu^{III} complexes measured in A) methanol and B) water. Concentration in solution of 1.0x10⁻⁵ mol·L⁻¹. All measurements were carried out with a bandpass of 2.5 nm for both Ex and Em, with an increment of 0.5 nm and an integration time of 0.5 s. 106
- Figure 42.** Vibrational coupling between the ⁵D₀ emitting level of the Eu^{III} ion and some of the most common quenching oscillators. A generic coordination sphere of Eu^{III} complex is inserted to illustrate the coordination of OH oscillators. 108

Figure 43. Excitation and emission spectra of Ir ^{III} -p, Ir ^{III} -Gd ^{III} , and Ir ^{III} -Eu ^{III} complexes measured in A) dichloromethane, and B) chloroform. Concentration in solution of 1.0x10 ⁻⁵ mol·L ⁻¹ . All measurements were carried out with a bandpass of 2.5 nm for both Ex and Em, with an increment of 0.5 nm and an integration time of 0.5 s.	110
Figure 44. i) Color-mixed LED based on the combination of three LED chips emitting blue, green, and red light; ii) phosphor-converted LED based on a near-UV-emitting LED chip coated with a mixture of phosphors; 3) hybrid LED based on the blue-emitting LED chip coated with a yellow-emitting phosphor. Hybrid LEDs are often called phosphor-converted LED as well [168].	115
Figure 45. Schematic representation of a p-n junction, showing the electron-hole recombination.	116
Figure 46. Timeline of our research group (LLuMeS) in application of SSL.	117
Figure 47. A) Excitation and B) emission spectra of Ir ^{III} -p doped films.	119
Figure 48. Excitation, and B) emission spectra of Ir ^{III} -p-doped films. C) Photographs of Ir ^{III} -Eu ^{III} -doped PMMA films acquired using an optical microscopy. ...	120
Figure 49. A) Emission spectra of the UV LED-chip used as the excitation source in blue, of Ir-p:LED prototype in green, and of the Ir-p-Eu:LED prototype in yellow. B) Radiant emission spectra obtained hour after hour for the Ir p-Eu:LED prototype. Inserted the energy diagram illustrating the energy decreasing in the donor state of the Ir-p in the fabricated prototype over time.	122
Figure 50. A) Emission spectra obtained hourly from the Ir-p:LED prototype, and B) Radiant stability of each UV LED prototype analyzed within 18 hours.	123
Figure 51. A) Normalized emission spectra obtained under different voltages from the Ir ^{III} -p:LED prototype, and B) Emission spectra obtained by varying the voltage applied to the Ir ^{III} -Eu ^{III} :LED prototype, from 2.90 V to 3.04 V. ...	123
Figure 52. A) Deconvolution of the emission spectra obtained at 3.00V of the Ir-p-Eu:LED prototype, B) linear fit of the Ir ^{III} /Eu ^{III} emission area ratio as a function of the energy of the maximum emission band of the Ir-p component in the Ir-p-Eu:LED prototype.	124

Figure 53. Schematic representation of the deactivation of triplet states of the phosphorescent molecule by oxygen using the simplified Jablonski diagram.	128
Figure 54. Schematic illustration of a ratiometric system (a) use of a dynamic luminophore or (b) two dynamic luminophores. Adapted from [209].	130
Figure 55. A) Isolated, B) germinal, and C) vicinal silanol groups on silica particles.	132
Figure 56. Timeline of our research group (LLuMeS) on the development of luminescent materials based on silica particles.	133
Figure 57. Schematic representation of SiO ₂ -Eu ^{III} Ir ^{III} synthetic route, the molecules and the particle are out of scale, and merely represent an illustration of the formation of the hybrid.	137
Figure 58. A) TEM image of SiO ₂ -Eu ^{III} Ir ^{III} particles and B) histogram of the size distribution.	138
Figure 59. Vibrational spectra of SiO ₂ (black), SiO ₂ -NCO (red), SiO ₂ -COOH (green), SiO ₂ -Eu (dark blue), and SiO ₂ -EuIr (light blue).	139
Figure 60. Experimental and theoretical ratios of C/N in the SiO ₂ -COOH, SiO ₂ -Eu ^{III} , and SiO ₂ -Eu ^{III} Ir ^{III} samples. *The degree of functionalization was determined using the carbon and nitrogen percentages of the SiO ₂ -COOH sample, since only organic matter was grafted onto it. In the estimation of the C/N ratio of SiO ₂ -Eu ^{III} Ir ^{III} was considered two Ir ^{III} complexes coordinated into the Eu ^{III} ion, in the illustration here presented, there is only one Ir ^{III} represented, for the sake of clarity.	140
Figure 61. Thermogravimetric curves of the silica samples.	141
Figure 62. Surface charge estimated by zeta potential of the SiO ₂ , SiO ₂ -NCO, SiO ₂ -COOH, SiO ₂ -Eu ^{III} , and SiO ₂ -Eu ^{III} Ir ^{III} samples.	142
Figure 63. A) Excitation spectra, B) emission spectra of SiO ₂ -Eu ^{III} and SiO ₂ -Eu ^{III} Ir ^{III} , and color diagram of SiO ₂ -Eu ^{III} and SiO ₂ -Eu ^{III} Ir ^{III} samples.	143
Figure 64. Schematic representation of Ir ^{III} moiety emission suppression in the SiO ₂ -Eu ^{III} Ir ^{III} hybrid.	144
Figure 65. Emission spectra obtained at different dissolved oxygen (DO) concentrations, and schematic representation of two main quenching channels to Ir ^{III}	145

Figure 66. Variation in the color perception represented by CIE 1931 2° color coordinates.....	146
Figure 67. Emission lifetime of the Ir ^{III} moiety in A) air and B) after purging nitrogen gas.....	147
Figure 68. A) Graphical representation of the Ir ^{III} /Eu ^{III} ratio with dissolved oxygen (DO) variation, and B) Stern-Volmer plot where I ₀ is the Ir ^{III} /Eu ^{III} ratio with 0 ppm DO, and I is the Ir ^{III} /Eu ^{III} ratio with different DO concentrations.	148
Figure 69. Cell viability of SiO ₂ -Eu ^{III} Ir ^{III} sample obtained from the Huh 7.5 cell line using MTT assays.	151
Figure 70. Confocal images of Huh cells incubated with SiO ₂ -Eu ^{III} Ir ^{III} sample (50 μg·mL ⁻¹). A) Nuclei stained with Hoechst dye; B) Ir ^{III} component emission; C) Eu ^{III} emission; D) merge of B and C images; E) merge of A and B images; F) merge of A and C images; and G) merge of E and F images.	152

List of tables

Table 1. Emission quantum yield of red, green, and blue emitters based on Ir ^{III} ion. λ_{em} is the maximum emission wavelength, and Φ is the emission quantum yield.	35
Table 2. Comparison of incandescent, fluorescent, LED, and OLED lamps [].	55
Table 3. Root mean square deviation (RMSD) between ground and excited states for each complex.	64
Table 4. Molecular orbital composition analysis (%) for each ligand and metal center. Molecular orbital composition analysis (%) for each ligand and metal center. Decomposition was performed through Mulliken-partition [] in MultiWFN software [].	69
Table 5. Molecular orbital composition analysis (%) for each ligand and metal center. Decomposition was performed through Mulliken-partition [134] in MultiWFN software [135].	71
Table 6. Molecular orbital composition analysis (%) for each ligand and metal center. The decomposition was performed using the Mulliken partition [134] in MultiWFN software [135].	73
Table 7. HOMO, LUMO, and energy difference between the HOMO and LUMO orbitals ($\Delta E = LUMO - HOMO$) of the complexes under study.	74
Table 8. Photophysical properties of N,N-(<i>trans</i>)-Ir ^{III} p and N,N-(<i>cis</i>)-Ir ^{III} p complexes measured in different solvents. Φ is the overall emission quantum yield, τ is the emission lifetime, kr is the radiative decay rate, and k_{nr} is the nonradiative decay rate.	78
Table 9. Photophysical properties of N,N-(<i>trans</i>)-Ir ^{III} m and N,N-(<i>cis</i>)-Ir ^{III} m complexes measured in different solvents. Φ is the overall emission quantum yield, τ is the emission lifetime, kr is the radiative decay rate, and k_{nr} is the nonradiative decay rate.	80
Table 10. Photophysical properties of N,N-(<i>trans</i>)-Ir ^{III} t and N,N-(<i>cis</i>)-Ir ^{III} t complexes measured in different solvents. Φ is the overall emission quantum yield, τ is the emission lifetime, kr is the radiative decay rate, and k_{nr} is the nonradiative decay rate.	82

Table 11. Photophysical properties of Ir ^{III} -p, Ir ^{III} -Gd ^{III} , and Ir ^{III} -Eu ^{III} complexes measured in ethyl acetate, acetonitrile (ACN), and DMSO. Φ is the overall emission quantum yield, τIr is the Ir ^{III} moiety lifetime, kr is the radiative decay rate, knr is the nonradiative decay rate, $\Phi EuEu$ is the intrinsic emission quantum yield, τEu is the emission lifetime, and A_r and A_{nr} are the radiative and nonradiative decay rates of the ⁵ D ₀ emissive state of Eu ^{III} ion. Concentration in solution of 1.0x10 ⁻⁵ mol·L ⁻¹	103
Table 12. Judd-Ofelt parameters (Ω_2 and Ω_4) and area ratio between emission bands related to ⁵ D ₀ → ⁷ F ₂ and ⁵ D ₀ → ⁷ F ₁ transitions.	105
Table 13. Photophysical properties of Ir ^{III} -p, Ir ^{III} -Gd ^{III} , and Ir ^{III} -Eu ^{III} complexes measured in methanol and water. Φ is the overall emission quantum yield, τIr is the Ir ^{III} moiety lifetime, kr is the radiative decay rate, knr is the nonradiative decay rate, $\Phi EuEu$ is the intrinsic emission quantum yield, τEu is the emission lifetime, and A_r and A_{nr} are the radiative and nonradiative decay rates of the ⁵ D ₀ emissive state of Eu ^{III} ion.....	107
Table 14. Judd-Ofelt parameters (Ω_2 and Ω_4) and area ratio between emission bands related to ⁵ D ₀ → ⁷ F ₂ and ⁵ D ₀ → ⁷ F ₁ transitions.	109
Table 15. Photophysical properties of Ir ^{III} -p, Ir ^{III} -Gd ^{III} , and Ir ^{III} -Eu ^{III} complexes measured in dichloromethane (DCM) and chloroform. Φ is the overall emission quantum yield, τIr is the Ir ^{III} moiety lifetime, kr is the radiative decay rate, knr is the nonradiative decay rate, $\Phi EuEu$ is the intrinsic emission quantum yield, τEu is the emission lifetime, and A_r and A_{nr} are the radiative and nonradiative decay rates of the ⁵ D ₀ emissive state of Eu ^{III} ion.....	111
Table 16. Judd-Ofelt parameters (Ω_2 and Ω_4) and area ratio between emission bands related to ⁵ D ₀ → ⁷ F ₂ and ⁵ D ₀ → ⁷ F ₁ transitions.	111
Table 17. Solvent properties and influence on the photoluminescent properties of Ir ^{III} -Eu ^{III} bimetallic complex studied in this work.	112
Table 18. Percentage values and ratio between carbon and nitrogen calculated (theo.) and found (exp.) for SiO ₂ -COOH, SiO ₂ -Eu ^{III} , and SiO ₂ -Eu ^{III} Ir ^{III} . .	140
Table 19. Photophysical results from SiO ₂ -Eu ^{III} and SiO ₂ -Eu ^{III} Ir ^{III} Samples.	143

LIST OF ABBREVIATIONS

¹LC	singlet ligand-centered transitions
¹LLCT	singlet ligand-to-ligand charge-transfer
¹MLCT	singlet metal-to-ligand charge-transfer
³LC	triplet ligand-centered transitions
³LLCT	triplet ligand-to-ligand charge-transfer
³MLCT	triplet metal-to-ligand charge-transfer
A	acceptor state
ATP	adenosine triphosphate
BC	Before Crist
BSA	bovine serum albumin protein
CCT	correlated color temperature
CFSE	Crystal Field Stabilization Energy
CPS	counts per seconds
CRI	color rendering index
D	donor state
DCL	down-conversion
DFT	density functional theory
DO	dissolved oxygen
EBL	electron blocking layer
EML	emissive layer
ET	energy transfer
ETL	electron transport layer
FED	forced electric dipole
FTIR	Fourier transformed infrared
HBL	hole blocking layer

HOMO	highest occupied molecular orbital
HTL	hole transport layer
IPTES	3-(triethoxysilyl)propyl isocyanate
ISC	intersystem crossing
ITO	indium-tin-oxide
LC	ligand-centered states
LE	luminous efficacy
LEDs	light-emitting diodes
Ln^{III}	Lanthanide ^{III}
LOD	limit of detection
LUMO	lowest unoccupied molecular orbital
MALDI	Matrix Assisted Laser Desorption/Ionization
MC	metal-centered states
MLCT	metal-to-ligand charge transfer states
MO	molecular orbital
MOFs	metal organic frameworks
MR	magnetic resonance
MTT	3-(4,5-dimethylthiazol-2-yl)-2,5-diphenyltetrazolium bromide
NIR	near-infrared
NMR	nuclear magnetic resonance
OLEDs	organic light-emitting diodes
PBS	Phosphate buffer saline
PET	photo-induced electron transfer
PLEDs	polymeric light-emitting diodes
RGB	Red, Green, and Blue
RMSD	Root mean square deviation
SMMs	Single-molecule magnets

SOC	Spin-orbit coupling
SSL	solid-state lighting
TD-DFT	time-dependent DFT
TEA	Tetraethylammonium
TEOS	silicon tetra alkyl orthosilicate
TEM	transmittance electronic microscopy
UCL	up-conversion luminescence
US	United States
WLED	white light-emitting diode

LIST OF SYMBOLS

λ_{em}	maximum emission wavelength
τ	emission lifetime
τ_{Eu}	emission lifetime of the europium ion
$\chi = n(n+2)^2/9$	correction of the local Lorentz field
Φ	emission quantum yield
Φ_{Eu}^{Eu}	intrinsic emission quantum yield
φ	luminous flux
δ	deformation
Ψ_T	total triplet wave function
$\langle \Psi_f U^{(\lambda)} \Psi_i \rangle$	double reduced elements
Ω_λ	Judd-Ofelt parameters
ω	angular frequency
A_{01}	spontaneous decay rate of the ${}^5D_0 \rightarrow {}^7F_1$ transition
A_{nr}	nonradiative decay rate of the europium ion
A_r	radiative decay rate of the europium ion
A_t	total decay rate
g	even (from the German <i>gerade</i>)
k_n	radiative decay rate
k_{nr}	nonradiative decay rate
n	refraction index
P_{out}	optical output power of the source
$S_{f \leftarrow i}$	oscillator strength
u	odd (from German <i>ungerade</i>)
v_{as}	antisymmetric stretching
v_s	symmetric stretching

Table of contents

Chapter 1	35
General introduction, statement of the problem, theory, and review of literature	35
1.1. Overview	35
1.2. Lanthanide Properties	37
1.3. Iridium ^{III} complexes	41
1.4. <i>d-f</i> heterobimetallic complexes.....	43
1.5. General aim of this Ph.D Thesis.....	46
1.6. Specific aims	46
1.7. Characterization techniques.....	46
1.8. References.....	48
Chapter 2	53
Ir^{III}-based complexes: Influence of the synthesis procedure on photoluminescent properties	53
2.1. Introduction	53
2.2. Experimental Procedure.....	61
2.3. Structural characterization.....	65
2.4. Theoretical calculations.....	69
2.5. Photoluminescence study	76
2.6. Conclusion	82
2.7. References.....	83
Chapter 3	88
Ir^{III}-Ln^{III} Heterobimetallic complexes: The sensitization process of the Eu^{III} ion	88
3.1. Introduction	88
3.2. Experimental Procedure.....	92
3.3. Structural characterization.....	93
3.4. Photoluminescence study	97
3.4.1. Non-protic polar solvents.....	100
3.4.2. Protic polar solvents	105
3.4.3. Non-polar solvents.....	109
3.5. Conclusions.....	112

3.6. References.....	112
Chapter 4.....	115
Heterobimetallic Iridium^{III}-Europium^{III} complex applied in PC-LEDs and the role of donor energy on sensitizing the Eu^{III} ion.....	115
4.1. Introduction.....	115
4.2. Experimental Procedure.....	118
4.3. PMMA film characterization.....	119
4.4. PC-LEDs prototypes characterization.....	121
4.5. Conclusions.....	125
4.6. References.....	125
Chapter 5.....	127
Silica particles decorated with Ir^{III}-Eu^{III} heterobimetallic complex for oxygen sensing: a luminescent, cytotoxic, and cell imaging study.....	127
5.1. Introduction.....	127
5.2. Experimental Procedure.....	135
5.3. Structural characterization.....	138
5.4. Photoluminescence study.....	142
5.5. Oxygen sensing.....	144
5.6. Cytotoxic study.....	150
5.7. Cell imaging study.....	151
5.8. Conclusions.....	153
5.9. References.....	154
Chapter 6.....	159
Final Remarks.....	159
6.1. General conclusion.....	159
6.2. Resumo expandido em português.....	161

Chapter 6

Final Remarks

6.1. General conclusion

The main goal of this Ph.D thesis was to synthesize, characterize *d*, *f*, and intermetallic complexes, study the influence of solvents in the sensitization process of the Eu^{III} ion from a $^3\text{MLCT}$ state, and then study their applicability as coating phosphors to create solid-state lighting devices, as dissolved oxygen probes, and as cell imaging dyes.

The influence of the synthesis parameters to obtain heteroleptic Ir^{III} complexes with different arrangements was efficient for anionic and neutral Ir^{III} -based complexes because the products obtained by different methodologies presented different spectroscopy properties. For cationic Ir^{III} -based complexes, both methodologies produced the same isomer, or both isomers displayed the same emission profile, however, additional characterizations are needed to fully elucidate the complex structures.

The spectroscopy studies performed to understand the sensitization process of the Eu^{III} ion in bimetallic complexes made it possible to rationalize some solvent properties that play an important role in this process. Highly polar solvents help Eu^{III} sensitization, demonstrating that even when the $^3\text{MLCT}$ donor state is low in energy, energy transfer is a favorable process; another important conclusion is that the energy of the $^3\text{MLCT}$ donor state is the most important parameter when performing luminescence measurements in nonpolar or low-polarity solvents, similar to the solid state.

The applicability of heterobimetallic $\text{Ir}^{\text{III}}\text{-Eu}^{\text{III}}$ complex in solid-state lighting devices was evaluated in comparison to a heteroleptic Ir^{III} -based complex. The complexes were immobilized in PMMA film. The $\text{Ir}^{\text{III}}\text{-Eu}^{\text{III}}$ bimetallic complex applied as a PC LED showed great radiant stability, losing only 15% of the initial intensity after 18 h of operation, compared with 28% of the Ir^{III} complex prototype. As the bare UV-LED loses approximately 13% of its initial area, it is pertinent to say that the decrease in the total emission area for the $\text{Ir}^{\text{III}}\text{-Eu}^{\text{III}}$:LED prototype is largely due to

the decrease in the efficiency of the commercial UV LED-chip used as the excitation source. In addition, with this study, it was possible to determine the minimum energy of the ligand triplet donor level to observe only the red emission of the Eu^{III} ion in a heterobimetallic Ir^{III}-Eu^{III} complex, i.e., 19,103 cm⁻¹.

With the aim of biological applications, Ir^{III}-Eu^{III} heterobimetallic complexes were grafted onto silica particles to overcome the low water solubility of the complexes and make them suitable for such applications. Structural characterizations confirmed the formation of spherical particles with an average size around 275±13 nm. The functionalization process was attested by elemental and thermal analysis, and by the zeta potential, the final hybrid showed a negative value of -14.20 mV, which is adequate to form a stable colloidal suspension. From the photoluminescent characterization, it was possible to attest to the dual-emission character of the material under study. The excitation band of the final hybrid extends from 250 nm to approximately 550 nm. This feature is crucial when bioapplication is intended because low excitation energy can be used to excite the luminescent probe, thereby avoiding possible damage to biotissues.

The luminescent silica particles were tested in oxygen sensing tests. Oxygen sensing measurements showed that the final hybrid has a nonlinear response to oxygen concentration. In contrast to what was expected, with the decrease in oxygen content, the Ir^{III} emission moiety exhibits a decrease in emission intensity compared with the Eu^{III} ion. This increase in the sensitization process can be attributed to the increase in the emission lifetime of the ³MLCT state because the electrons that populate the ³MLCT state of the Ir^{III} moiety have more time to migrate to the ⁵D₀ or ⁵D₁ level of the Eu^{III} ion.

Toxicity assays were performed using the Huh-7.5 cell line, and the SiO₂-Eu^{III}Ir^{III} nanoparticles were nontoxic at concentrations between 1.56 and 400 µg·mL⁻¹. The cells were incubated for 4 h with a suspension of 50 µg·mL⁻¹ to obtain confocal microscopy images. The images prove that the nanoparticles were internalized by the cells, maintaining their luminescent properties because green and red emissions were separately detected using different laser excitations.

6.2. Resumo expandido em português

Dados da literatura mostram uma correlação entre a eficiência de emissão e a energia do comprimento de onda máximo de emissão de um luminóforo. Normalmente, quanto mais deslocado para o vermelho for a emissão, menor será o rendimento quântico, o que é explicado pela lei do *gap* de energia. Assim, os emissores vermelhos normalmente têm rendimentos quânticos de emissão mais baixos do que os emissores azuis ou verdes. Isto mostra a importância da investigação centrada na síntese de novos compostos emissores no vermelho, objetivando o melhoramento do rendimento quântico de emissão, tornando-os comparáveis aos emissores azuis e verdes em termos de eficiência. As três cores citadas acima podem formar um sistema denominado RGB (do inglês *Red*, *Green*, e *Blue*), no qual, através da modulação da emissão dessas três cores fundamentais da luz, pode-se gerar praticamente qualquer cor luz. Este sistema é utilizado para toda produção de luz que requeira modulação de cores e eventualmente para criação de luz branca, seja para iluminação, fins decorativos ou aplicações em telas e *displays* de dispositivos eletrônicos.

Tais emissores vermelhos não são importantes apenas para aplicações tecnológicas, mas também para ensaios biológicos como corantes de imagem ou sensores, uma vez que a emissão de tais luminóforos pode ser distinguida da autofluorescência do meio biológico, que ocorre nas regiões azul e verde. Além disso, a luz vermelha é menos absorvida pelo sangue, gordura e pele. Dessa forma, à medida que menos fótons vermelhos e infravermelhos são absorvidos pelo corpo, mais fótons chegam ao detector e respostas mais confiáveis podem ser obtidas por meio de imagens. O uso de sondas luminescentes para analisar variáveis em meios biológicos, como a concentração de O₂ dissolvido, é muito útil no diagnóstico de algumas doenças, pois alterações nas concentrações podem indicar estados patológicos que podem resultar em alterações celulares e/ou morte de todo o organismo. Visando as duas aplicações citadas, iluminação e detecção de oxigênio em meio biológico, nesta tese de doutorado foram realizadas sínteses e estudos espectroscópicos de novos complexos luminescentes de Ir^{III}, Eu^{III}, e Ir^{III}-Ln^{III} ancorados ou não em partículas de sílica.

O íon európio^{III} foi escolhido porque as transições *f-f* nos íons lantanídeos fornecem uma propriedade única de emissão de luz. Os orbitais *4f* são protegidos sofrendo pouca influência do ambiente químico externo, o que resulta em bandas estreitas de emissão com alta pureza de cor. As cores referentes à emissão de íons lantanídeos variam de acordo com a posição energética dos níveis, que por sua vez depende do preenchimento do orbital *4f*. O íon Eu^{III}, por exemplo, exibe uma emissão característica na região vermelha. Entretanto, explorar as propriedades luminescentes desses íons é difícil porque eles apresentam baixa absorvidade molar (em torno de 10 L·mol⁻¹·cm⁻¹), típica das transições *f-f* que são proibidas, principalmente pela regra de seleção de Laporte e, em alguns casos, também pela de spin.

Para superar o problema da baixa absorvidade molar imposta aos íons lantanídeos pelas regras de seleção, uma alternativa é coordenar moléculas orgânicas, ou complexos metálicos do bloco *d* em íons lantanídeos, que possuem maior absorvidade molar e são capazes de transferir a energia absorvida para o íon lantanídeo. Este mecanismo de sensibilização é comumente conhecido como "efeito antena". Essa sensibilização pode ser completa ou parcial, dependendo da diferença de energia entre os níveis do doador e do aceitador.

No capítulo 2, é discutido a síntese de complexos de Ir^{III} que posteriormente poderão ser utilizados na síntese de complexos heterobimetálicos do tipo *d-f*. Considerando que diferentes metodologias para sintetizar complexos bis-ciclometalados de Ir^{III} podem influenciar o arranjo químico dos átomos, produzindo diferentes isômeros, foi apresentada a síntese de três pares de isômeros *trans-cis*, e estudada a influência da metodologia sintética em suas propriedades luminescentes. Para este propósito, um dímero precursor de Ir^{III} foi sintetizado através da rota de Nonoyama usando o ligante ciclometalante 2-(2,4-difluorofenil)piridina (dfppy). O ligante dfppy foi escolhido por sua grande separação entre os orbitais HOMO e LUMO, o que resulta na emissão deslocada para o azul em comparação com outros ligantes ciclometalantes regularmente usados. Após, os complexos heteroléticos baseados em Ir^{III} foram sintetizados utilizando duas metodologias diferentes. O isômero *trans* foi sintetizado à temperatura ambiente e o isômero *cis* a 110°C sob sistema de refluxo. Os ligantes ancilares foram escolhidos para sintetizar complexos com diferentes cargas. Primeiro, o ligante ácido 2,2'-bipiridina-3,3'-dicarboxílico (bpdc) resultou em complexos aniônicos, o ligante ácido

pirimidina-2-carboxílico (pmc) em complexos neutros e, finalmente, o ligante 2,4,6-tris(2-piridil)-s-triazina (tptz) resultou em complexos carregados positivamente. Além disso, estes ligantes ancilares também foram escolhidos para formar complexos heterolépticos de Ir^{III} com um segundo sítio de coordenação, que pode então ser usado para sintetizar complexos bimetálicos coordenando íons Ln^{III} ou outros íons do bloco *d*. Através das caracterizações estruturais experimentais (FTIR e MALDI), foi possível concluir que os complexos foram formados com as estequiometrias propostas entre os ligantes ciclometalantes dfppy e os ligantes ancilares (bpdc, pmc e tptz), porém, medidas de RMN de ¹H ou monocristais não foram obtidos, e os arranjos corretos dos isômeros não foram elucidadas experimentalmente. Assim, a elucidação de cada isômero foi suportada por cálculos DFT. Os espectros de absorção e emissão foram simulados e posteriormente comparados com aqueles obtidos experimentalmente, os quais apresentaram boa concordância. O primeiro par de isômeros, N,N-(*trans-cis*)-Ir^{III}p com carga negativa, apresentou propriedades fotoluminescentes distintas entre os isômeros. O isômero N,N-(*cis*)-Ir^{III}p apresentou emissão localizada em maior energia com maiores rendimentos quânticos de emissão e tempos de vida em todos os solventes testados. O par de isômeros N,N-(*trans-cis*)-Ir^{III}m, o par neutro, apresentou perfil de emissão diferente entre os isômeros, sendo que o isômero *cis* novamente apresentou emissão mais deslocada para o azul, entretanto, valores semelhantes de rendimento quântico de emissão e tempo de vida foram observados para ambos os isômeros em todos os solventes testados. O último par de isômeros, N,N-(*trans-cis*)-Ir^{III}t, de carga positiva, apresentou espectros de excitação e emissão semelhantes entre os isômeros, com valores semelhantes de rendimento quântico de emissão e tempo de vida, indicando que os diferentes arranjos não influenciam as propriedades fotofísicas deste tipo de complexo, ou indicando que apenas um isômero foi obtido através de ambas as metodologias.

No capítulo 3 dois novos complexos bimetálicos de Ir^{III}-Ln^{III} (Ln^{III} = Gd^{III} e Eu^{III}) foram sintetizados, nos quais foi analisada a influência dos solventes nas propriedades luminescentes. O complexo de Ir^{III} utilizado para sintetizar os complexos bimetálicos foi selecionado por análises das propriedades fotofísicas dos complexos de Ir^{III} estudados no Capítulo 2. Energeticamente, o complexo mais adequado para sensibilizar o íon Eu^{III} é N,N-*cis*-[Ir(dfppy)₂(bpdc)], pois apresentou emissão em maior energia entre os complexos de Ir^{III} estudados. Porém, após

diversas tentativas de sintetizar complexos bimetálicos através de metodologias úmidas e hidrotérmicas, nenhum sistema bimetálico foi obtido com esse isômero. Portanto, o complexo N,N-*trans*-[Ir(dfppy)₂(bpdc)] foi utilizado como ligante. No capítulo 3, o complexo N,N-*trans*-[Ir(dfppy)₂(bpdc)] foi denominado como Ir^{III}-p. Através dos estudos espectroscópicos realizados neste capítulo, foi possível concluir que alguns propriedades dos solventes auxiliam no processo de transferência de energia e melhoram as propriedades luminescentes em solução de complexos bimetálicos Ir^{III}-Eu^{III}:

(i) Solventes altamente polares desempenham um papel importante na sensibilização de Eu^{III}, demonstrando que mesmo quando o estado doador ³MLCT está situado em região de baixa energia, a sensibilização é um processo favorável;

(ii) A energia do estado doador ³MLCT é o parâmetro mais importante no processo de sensibilização ao realizar medida em solventes de baixa polaridade;

(iii) Os solventes não coordenantes aumentam moderadamente os valores de rendimento quântico de emissão comparados com solventes coordenantes com osciladores OH. No entanto, a coordenação de moléculas de solvente livres de osciladores OH aumenta grandemente os rendimentos quânticos de emissão, e especialmente o rendimento quântico intrínseco do íon Eu^{III}.

(iv) Finalmente, os solventes com osciladores OH são fortes supressores da luminescência Eu^{III}.

O complexo bimetálico Ir^{III}-Eu^{III} apresentado no Capítulo 3 apresentou emissão amarelo-laranja no estado sólido, sugerindo que em um sistema rígido, como por exemplo, imobilizado em filmes poliméricos, pode ocorrer transferência parcial de energia, e um perfil de espectro de emissão semelhante deve ser obtido. Assim, no capítulo 4, é relatado a preparação de filmes de PMMA emissores no amarelo para aplicação em iluminação de estado sólido. O polímero PMMA foi escolhido por apresentar as melhores qualidades quando aplicado para imobilizar complexos luminescentes, como transparência de absorção na região espectral do visível e atuar como guia de onda. O complexo bimetálico Ir^{III}-Eu^{III} aplicado como PC LED apresentou boa estabilidade radiante, perdendo apenas 15% da intensidade inicial após 18 h de operação. No entanto, o comprimento de onda de emissão dominante apresentou deslocamento para o vermelho devido aquecimento durante o tempo de operação, e, portanto, diminuindo a energia do estado doador ³MLCT do componente Ir^{III}, reduzindo a eficiência do processo de sensibilização ao íon Eu^{III}.

Além disso, com este estudo foi possível determinar a energia mínima do nível tripleto doador do ligante para observar apenas a emissão vermelha do íon Eu^{III} em um complexo heterobimetálico $\text{Ir}^{\text{III}}\text{-Eu}^{\text{III}}$, que foi calculada em 19.103 cm^{-1} . Com este resultado é possível prever se um complexo heteroléptico de irídio tem energia suficiente para sensibilizar eficientemente o íon Eu^{III} para produzir compostos com alta pureza de cor na região do vermelho.

No capítulo 5, partículas de sílica decoradas com complexos heterobimetálicos de $\text{Ir}^{\text{III}}\text{-Eu}^{\text{III}}$ para detecção de oxigênio foram estudadas. As caracterizações estruturais confirmaram a formação de partículas esféricas com tamanho médio em torno de $275 \pm 13 \text{ nm}$. O processo de funcionalização foi confirmado por análise elementar e térmica, e por potencial zeta, o híbrido final apresentou valor negativo de $-14,20 \text{ mV}$, o que é adequado para formar uma suspensão coloidal estável. A partir da caracterização fotoluminescente foi possível atestar a natureza dual de emissão do material em estudo, apresentando uma banda larga de emissão na região do verde proveniente do complexo ligante de Ir^{III} , e bandas estreitas de emissão do íon Eu^{III} na região espectral vermelha. A banda de excitação do híbrido final estende-se de 250 nm a aproximadamente 550 nm . Esta característica é crucial quando se pretende aplicação em meio biológico, já que baixa energia de excitação pode ser usada para excitar a sonda luminescente, evitando possíveis danos aos tecidos.

As medições de detecção de oxigênio mostraram que o híbrido final tem uma resposta não linear à concentração de oxigênio. Para entender o processo de desativação foi utilizado o modelo de Ster-Volmer de dois sítios, e assim ficou evidente uma enorme heterogeneidade do material, pois dois sítios diferentes foram ajustados com aproximadamente 50% cada, porém diferentes constantes de desativação foram determinadas, mostrando que os sítios apresentam diferentes sensibilidades às moléculas de oxigênio. Ao contrário do que seria esperado, com a diminuição do teor de oxigênio, a emissão do complexo de Ir^{III} apresenta uma diminuição na intensidade de emissão em comparação ao íon Eu^{III} . A diminuição do teor de oxigênio aumenta o processo de sensibilização ao íon Eu^{III} . Em altas concentrações de oxigênio, a excitação do estado $^3\text{MLCT}$ é extinta por interação com moléculas de oxigênio. Uma vez removidas as moléculas de oxigênio, os elétrons excitados no estado $^3\text{MLCT}$ podem ser transferidos para o estado emissivo do íon Eu^{III} , aumentando assim a intensidade relativa desta banda em comparação com a

emissão verde do Ir^{III}. Este aumento no processo de sensibilização pode ser atribuído ao aumento no tempo de vida da emissão do estado ³MLCT porque os elétrons que populam o estado ³MLCT do complexo de Ir^{III} têm mais tempo para migrar para o nível ⁵D₀ ou ⁵D₁ do íon Eu^{III}, aumentando assim a probabilidade de a sensibilização ocorrer. Além disso, medindo o tempo de vida, foi possível concluir que o principal mecanismo de extinção neste sistema é o mecanismo dinâmico. O híbrido final apresentou sensibilidade ao oxigênio de 70,5%, valor inferior aos valores já relatados na literatura para sistemas baseados em Ir^{III} ou outros sistemas monometálicos. Porém, é importante mencionar que esta é a primeira vez que partículas de sílica decoradas com sistemas bimetálicos *d-f* foram aplicadas para quantificar a concentração de oxigênio dissolvido. Desta forma, o presente trabalho ajudará a compreender e propor novos materiais voltados à detecção de oxigênio.

Os testes de toxicidade foram realizados utilizando a linhagem celular Huh-7.5, e as nanopartículas de SiO₂-Eu^{III}Ir^{III} não foram tóxicas em concentrações entre 1,56 e 400 µg·mL⁻¹. As células foram incubadas por 4 h com suspensão de 50 µg·mL⁻¹ para obtenção de imagens de microscopia confocal. As imagens comprovam que as nanopartículas foram internalizadas pelas células, mantendo suas propriedades luminescentes porque as emissões verdes e vermelhas foram detectadas separadamente através de excitação em mesmo comprimento de onda. Estes resultados mostram que este material é uma sonda luminescente ratiométrica promissora para marcação celular e detecção de oxigênio em meio biológico.